INVESTIGATION ON LOW NI DUPLEX STAINLESS STEEL GRADES

I. Calliari[1], J. Dobranszky[2], E. Ramous[1], G. Straffelini[3], G. Rebuffi[1]

[1]DIMEG University of Padua, Italy, [2]Hungarian Academy of Sciences, Hungary, [3]DIMTI University of Trento, Italy

Abstract

Different stainless steels (SS) can provide a very wide range of mechanical properties with the advantage of no need for surface protection. Duplex stainless steels (DSS), in particular, with twice the mechanical strength of conventional austenitic and ferritic SS, have a potential use in constructions. The DSS grades have been improved and, parallel with development towards higher grades for corrosive conditions, there is a great interest in leaner composition. A useful way to reduce the cost is to reduce the Ni content and to compensate with manganese and nitrogen additions. In the present paper the structural and mechanical properties of two low Ni duplex grades are compared in order to investigate the structural stability of the austenite as it may convert to martensite and the secondary phases precipitation. The detailed characterization has been performed with SEM-EDS and Charpy test on as received and on thermally treated (600-850°C) specimens. A few precipitates of chromium carbides and nitrides at the grain boundaries have been detected in both grades. The martensite structure has been noted only in 2101 type DSS. As concerns the impact toughness the behaviour of 2101 grade is quite similar to that of other DSS, while the 2304 has no drastic drop of toughness. Their corrosion properties in aggressive chloride environments are quite similar to that of austenitic AISI 304 grade.

Introduction

The good corrosion resistance of duplex stainless steels justify their applications in very aggressive environments, typical of chemical, offshore, oil and gas industries while their mechanical strength enables interesting applications both for constructions and transport vehicles, offering the advantage of reduced maintenance costs, being unnecessary the surface protection.

The base cost of the alloy is becoming a conditioning feature in diffuse and quantitatively important applications, in medium level aggressive environments. A great interest to develop lean grades of DSS aimed at the reduction of the cost, maintaining the basic good properties: mechanical strength, weldability, formability and good even if not extreme, corrosion resistance is growing.

An apparent way to reduce the alloy's cost is to reduce the content of the most expensive alloy components: nickel and molybdenum. Such reduction could be compensated by the increase of the manganese a nitrogen contents, to maintain the typical balanced microstructure of DSS, with both ferrite and austenite.

In the last decade research [1-4] has been carried out with the aim to define the composition of steel following the above criteria. Several different magnetic measurements were applied successfully to characterize the properties and the microstructure of duplex stainless steels [5, 6]. The main matters arise in maintaining the correct balance between ferrite and austenite contents and in the stability of the austenite against its transformation to martensite during cold forming

as a result of plastic deformation [1, 2]. For some years duplex grades with low Ni or Mn-N substitution for Ni have been proposed and are currently used, but a lack of information exist on structural stability after deformation or thermal treating.
The present paper is aimed to analyse the microstructure of two typical lean DSS.

Experimental

The as received materials were wrought rods (30 mm) previously solubilised (1050°C, 30 min), with chemical compositions lying in the ranges of Table 1.

Table 1. Chemical composition (%wt.).

Grade	C	Si	Mn	Cr	Ni	Mo	P	S	N
2101	0.030	0.60-0.80	4.0-5.0	22.0-0.5	1.0-1.5	0.50	0.035	0.005	0.19-0.22
2304	0.03	0.56	1.4	23.2	4.3	0.18	0.027	0.001	0.10

Isothermal "short" ageing treatments of specimens, were carried out at temperatures 550-850°C for 15-90 min and "long" treatment were carried out at 670 °C for 15-200 h.
The volume fractions of ferrite and austenite in a solution treated sample have been measured on 3 longitudinal and 3 transversal sections (20 fields for each section) by image analysis on light micrographs at 200×, after etching with the Beraha's reagent (reaction time, 10s).
The martensite which has been detected by OM and SEM, after etching with Beraha's reagent and by X ray diffraction (CrKα radiation).
Different phases have been observed by SEM examination of polished samples, using the backscattered electron (BSE) signal, on the basis of atomic number contrast effect: the ferrite appears slightly darker than austenite, while the secondary phases would appears lighter. The SEM operated at 25 kV; the BSE detector was set to maximize the atomic number contrast, allowing ferrite, austenite and other phases to be identified.
Instrumented Charpy–V impact specimens were prepared in the standard form of 10×10×55 mm. Impact test was carried out at room temperature, on samples treated at 550-650-750 and 850°C for 15-45-90 and 120 min.

Results and discussion

Solution treated material

The banded structure of elongated γ islands is observed in the longitudinal section, while the isotropic structure of ferrite and austenite grains is displayed on the transverse section. No secondary phases were detected. The values of volume fractions of ferrite and austenite, measured on longitudinal and transverse sections (200×), are reported in Table 2.

Table 2. Austenite (γ) and ferrite (α) % vol. in longitudinal and transverse sections.

	γ %2101	γ %2304	α %2101	α %2304
Longitudinal	50 ±2	56 ±2	50 ±2	53 ±3
Transverse	46±3	44±3	54±3	47±5

Table 3 reports chemical composition of ferrite and austenite measured with EDS-analysis, expressed as partition coefficients.
The Ni and Mn austenite enrichment and Cr ferrite enrichment are evident, the partition coefficients are quite similar to that observed in the common Cr-Ni-Mo grades.

Table 3. Austenite and ferrite compositions. (Wt %, EDS)

	α/γ 2304	**α/γ 2101**
Cr	1.23	1,14
Mn	0.75	0,84
Ni	0.59	0,62

Heat-treated samples

Microstructure of 2101 grade DSS

The microstructure has been investigated mainly on not-etched specimens by SEM-BSE; the ferrite is darker than austenite. At the temperature of 600°C, for treatment time < 40 min no precipitation of secondary phases has been detected, for longer times some small dark particles were detected at the ferrite grain boundaries. They were analyzed by SEM-EDS (close to the resolution limit) and an enrichment of Cr was observed at the grain boundaries so the precipitates were identified as chromium nitrides.
The same grain boundaries precipitation was observed after soaking times longer than 40min at 650°C, while at 750°C the first grain boundary precipitation has been detected after a 20 min treatment (Figure1a) and can still be observed after 20 h (Figure1b). Increasing the temperature, particles became larger and the precipitation occurs also at the α-γ boundaries (Figure 1b).

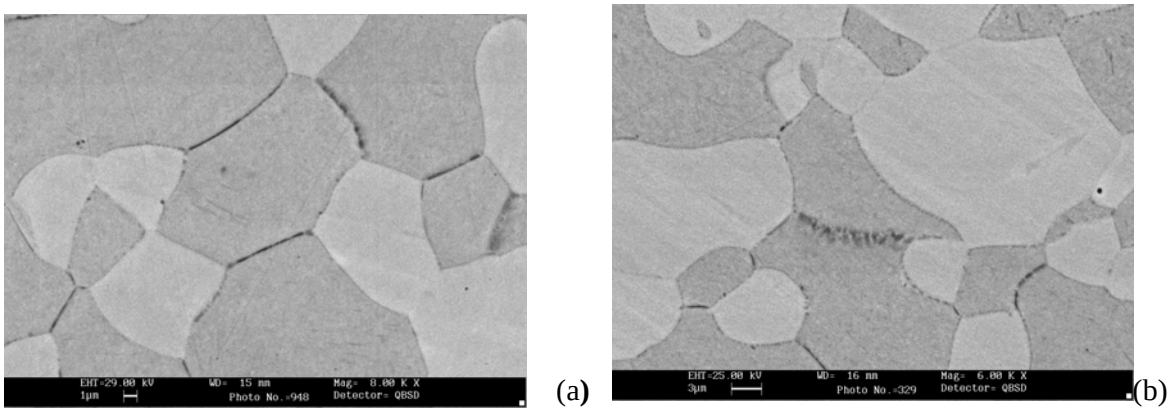

(a) (b)

Figure 1. SEM-BSE micrographs of sample treated at 750 °C for 45 min (a) and 20 h (b)

The shortest times for grain boundary carbide precipitation lies in the temperature range 650-750°C, as already observed [3].
No σ and χ phases have been detected, neither for very long thermal treatments in the 650-900 temperature range. This could be related to the low Ni and Mo contents.
In addition the Ni content may induce the instability of the austenite, as suggested in previous researches, which report of a probable transformation to martensite during cold forming (1). Moreover the martensite formation has been confirmed (2) in some low-Ni DSS after cold rolling and annealing (1040°C, air quenched).
We have detected different amount of martensite laths (Figures 2 and 3) in treated and rapidly quenched from 750-850°C samples. Different cooling rates have no significant effect on the amount of final martensite.
The X-ray diffraction spectra evidenced that the ferrite peaks increase as the amount of martensite increases**.**

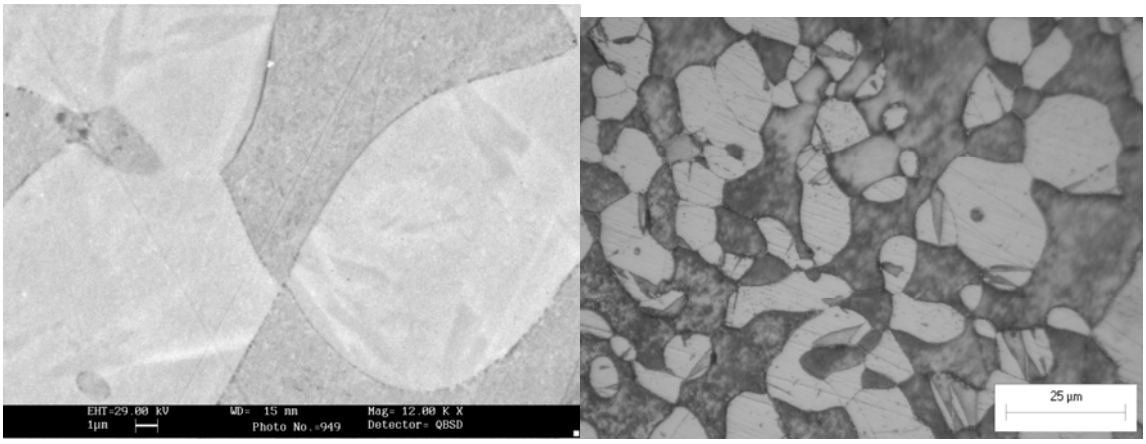

Figure 2. SEM-BSE and OM micrograph (750 °C, 25 min, WQ): martensite laths.

Microstructure of 2304 grade DSS

The microstructure of the 2304 grade DSS is not affected by the heat treatment at 600°C and no secondary phases or alpha-ferrite spinodal decomposition have been noted. A moderate precipitation of carbo-nitrides has been detected after long treatments (100 hours) at 670°C and after 45 min at 750°C.

In Figure 3 the SEM-BSE micrographs of the specimen treated for 90 min and 20 hours are reported. The carbo-nitride precipitation is evident just below the austenite grain boundary, as it has moved towards the austenite (ferrite) giving the precipitation inside the austenite grains.

A similar grain boundary precipitation was observed after long times (10 hours) treatment at 850°C but the kinetics are slower than at 750°C. On the other hand the main effect of the heat treatment in the range 600-850°C is the increasing of the austenite volume fraction, with values ranging from 44±1% of the as received sample to 62±2% of the sample treated at 850°C for 15 hours, accompanied by a decreasing of the Cr content in the austenite and by its increasing in the ferrite. This Cr enrichment and the very low amount of Mo seem to stabilize the ferrite and the secondary phases formation is not favoured.

The austenite of this grade appears to be stabile, indeed no austenite to martensite transformation has been detected after heat treatment. Probably the Ni (4.3%) and N (0.18%) contents are high enough to stabilize the austenite avoiding the structural transformation evidenced in the 2101 grade DSS.

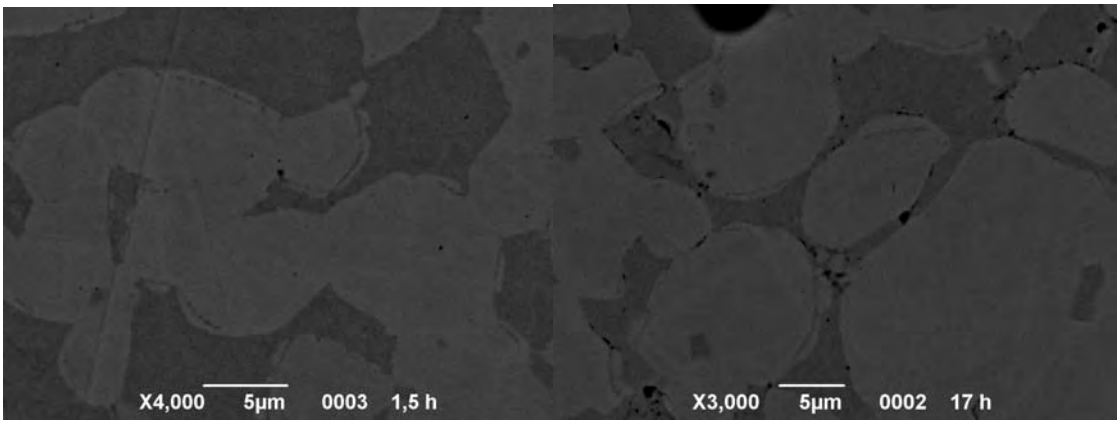

Figure 3. SEM-BSE micrographs: 750°C for 90min(left) and 20 hours(right)

Impact toughness

The effect of heat treatments on toughness of both the grades was studied by Charpy impact tests carried out at room temperature.
As shown in Figures 4 and 5, the steels have different impact toughness properties: the 2101 grade has the ductile and fragile behaviour, while the 2304 has no the fragile behaviour.
The 2101 is ductile until 20-40 minutes of isothermal treatment at 600-650°C, corresponding to first stages of the carbides-nitrides precipitation, where the impact energy drops down at about 50 J. The critical times for precipitation lie around 750°C, in good agreement with (3).
However the impact energy is never lower than 30 J, also after very long soaking times, of several hours. The presence of some laths of martensite on the impact toughness has not yet been investigated. The 2304 grade DSS is always ductile, with the impact energy values never lower than 200 J.
At this stage of the research we may conclude that the presence of nitrides at the austenite grain boundaries has no remarkable effects on the toughness of the 2304 steel.
The sample was treated at 550°C (1), 650°C (2), 750°C (3), 850°C (4), for 15 min (A), 45 min (B), 90 min (C), 120 min (D).

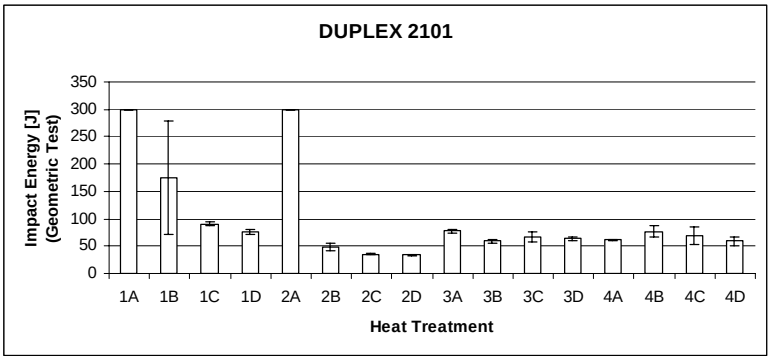

Figure 4. Impact energy of 2101 versus time/temperature of treatment

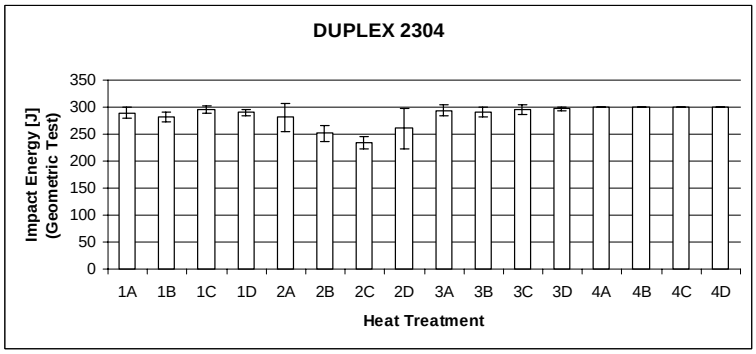

Figure 5. Impact energy for 2304 grade DSS versus time/temperature of heat treatment

Conclusions

Some results about the study of two duplex stainless steels with different low nickel contents were presented:

- The relatively low nickel and molybdenum contents make the precipitation of intermetallic phases more sluggish than in conventional duplex stainless steels, and no sigma related phases precipitation has been detected, also after long time isothermal aging treatments, in both the grades

- Precipitation at the grain boundaries of chromium nitrides has been observed after isothermal treatment in the temperature range 600-750°C, with different kinetics
- The austenite of the 2101 type DSS is quite instable, and a diffuse transformation austenite-martensite has been evidenced, while the austenite of the 2304 DSS is more stable and no martensite has been detected.
- The impact toughness after solution treatment is very good in both grades,
- The impact energy after isothermal treatment in the 2101 grade is never lower than 30 J, while in the 2304 is never lower than 200 J,
- General corrosion properties in chloride environments are quite similar to that of austenitic AISI 304 grades.

References

[1] C.D. Van Lelyveld, A. Van Benekom, Mater. Sci. Eng., A 204 (1996) p. 229.
[2] J.M. Hauser et al., Stainless Steel ’99, Science and Market, Sardinia, Italy, (1999), p. 85.
[3] P. Johansson, M. Liljas, AvestaPolarit Corrosion Management and Application Engineering, 24 (2002) p. 17.
[4] H. Sieurin, R. Sandstrom, E.L. Westin, Met. Mat. Trans. A, 37A (2006) p. 2975
[5] I. Mészáros, Physica B, 372 (2006) p. 181
[6] I. Mészáros, P.J. Szabó:, Journal of NDT&E International, 38 (2005) 7, p. 517

DUPLEX STAINLESS STEEL WELDS: RESIDUAL STRESS DETERMINATION, MAGNETIC FORCE MICROSCOPY AND SUSCEPTIBILITY TO INTERGRANULAR CORROSION

B. Gideon[1], L. Ward[2], D.G. Carr[3], O. Muransky[3]

[1]ARV Offshore, Thailand, [2]RMIT University, Australia, [3]Australian Nuclear Science and Technology Organization (ANSTO), Australia

Abstract

A section of a Duplex Stainless Steel (DSS) pipeline girth weld (single vee joint configuration) was systematically analyzed to determine the stress / strain levels and correlation with susceptibility to IGC within austenite and ferrite phases in the weld cap, fill and root region. Stress / strain levels were determined by means of Neutron Diffraction techniques. Magnetic Force Microscopy (MFM) were used to determine the size, shape and distribution of the austenite and ferrite within the various regions. ASTM A262 and a modified Double Loop Electrochemical Potentiokinetic Reactivation (DL-EPR) Test methods were used to assess the susceptibility to IGC. A clear variation of stress/strain was evident between the austenite and ferrite in the base material, HAZ and weld from the neutron diffraction results obtained. The results of the weld metal from MFM shows the formation of both a finer and coarse structure within the weld metal, which is dependent on the level of undercooling. The values for Ir/Ia and Qr/Qa in the DL-ERP test results revealed that the fill area had the highest level of susceptibility to IGC.

Keywords: Duplex Stainless Steel, Intergranular Corrosion, Double Loop Electrochemical Potentiokinetic Reactivation, Magnetic Force Microscopy, Neutron Diffraction

Introduction

Welding of Duplex Stainless Steel (DSS) is particularly difficult with respect to maintaining a ferrite–austenite ratio close to 50:50. Rapid cooling effects associated with weld thermal cycles, often results in ferrite contents in the weld metal in excess of 50% may result in the loss of strength and increased susceptibility to IGC. The weld structure and the austenite / ferrite phase ratio are largely influenced by weld heat inputs and the cooling rates.

The aim of this study is to conduct a detailed analysis of a girth welded sections of a DSS pipeline, as a function of heat input and type of weld, in terms of the residual stress by neutron diffraction, metallurgical analysis by means of magnetic force microscopy, and to assess the susceptibility to IGC by means of ASTM A262 and a modified Double Loop Electrochemical Potentiokinetic Reactivation (DL-EPR) test.

Experimental Procedures

Welding Conditions

The DSS linepipe wall thickness was 10mm with a 200mm diameter of UNS 31803. Full details are listed in Table 1.

Table 1. Chemical composition of pipe and filler material.

	C	Mn	P	S	Si	Ni	Cr	Mo	N	Cu	Cr_{eq}	Ni_{eq}
Pipe	0.030	2.0	0.025	0.015	1.0	6.50	23.00	5.50	0.20	0.16	32.04	10.78
Filler Material	0.016	1.69	-	-	0.42	8.60	23.07	3.20	0.160	0.16	28.09	11.90

Note; Cr_{eq} = Cr+1.37Mo+1.5Si+2Nb+3Ti and Ni_{eg} = Ni+22C+0.31Mn+14.2N+Cu

Manual Gas Tungsten Arc Welding (GTAW) technique was performed as detailed in Table 2. Upon completion of welding, the weld was subjected to Non Destructive Testing.

Table 2. Weld Condition – Single Vee joint configuration

Weld Pass	***Travel Speed***	***Heat Input***
	mm/min	***J/min***
1 (weld root)	51.00	1474.71
2 (weld fill)	123.00	883.12
3 (weld fill)	66.00	1745.45
4 (weld fill)	64.00	1788.00
5 (weld cap)	64.00	1685.63
	Average	1515.38

Residual Stress Measurements

Residual strain measurements were made using neutron diffraction with a wavelength of 1.40Å on TASS (The Australian Strain Scanner) at the Australian Nuclear Science Technology Organization (ANSTO), Strains were measured in the three directions - longitudinal, transverse and normal (L,T and N) to the welding direction. These were the assumed principal stress directions.

The measurement of residual elastic strain by monochromatic neutron diffraction relies on the use of Bragg's law to relate the lattice spacings, d_{hkl}, to the angle of diffraction $2\theta_{hkl}$ associated with the diffraction peak labeled by Miller indices *hkl* at a fixed wavelength. Strain was calculated from the selected planar atomic spacing for ferrite and austenite at discrete locations in the weldment using Eq. 1.

$$\varepsilon_{hkl} = (d_{hkl} - d^0_{hkl}) / d^0_{hkl} \quad (1)$$

The calculation of the residual strains requires the knowledge of an appropriate reference lattice spacing d^0_{hkl}. This is problematic in welds where there is a possibility of redistribution of alloying elements, and secondly, inhomogeneous plastic deformation across the weld will generate relatively strong intergranular stresses in DSS. This problem was addressed by cutting a companion slice 2mm thick from the weld and cutting slits every 2mm across it's length in order to relieve the macroscopic residual stress field. Thus, the reference measurements d^0_{hkl} represented the lattice spacing as a function of position relative to the weld centre and included any effects of alloy diffusion and intergranular stresses.

The average phase stress was calculated in the L,T and N directions for ferrite and austenite using the generalized Hooke's law:

$$\bar{\sigma}_L^{phase} = \frac{E_{hkl}}{(1+\nu_{hkl})(1-2\nu_{hkl})}\left[(1-\nu_{hkl})\varepsilon_L^{phase} + \nu_{hkl}\left(\varepsilon_T^{phase} + \varepsilon_N^{phase}\right)\right]$$
$$\bar{\sigma}_T^{phase} = \frac{E_{hkl}}{(1+\nu_{hkl})(1-2\nu_{hkl})}\left[(1-\nu_{hkl})\varepsilon_T^{phase} + \nu_{hkl}\left(\varepsilon_L^{phase} + \varepsilon_N^{phase}\right)\right] \quad (2)$$
$$\bar{\sigma}_N^{phase} = \frac{E_{hkl}}{(1+\nu_{hkl})(1-2\nu_{hkl})}\left[(1-\nu_{hkl})\varepsilon_N^{phase} + \nu_{hkl}\left(\varepsilon_T^{phase} + \varepsilon_L^{phase}\right)\right]$$

Where E_{hkl} and v_{hkl} and the diffraction elastic constants for each phase. The macroscopic residual stress field was then calculated by weighing the contribution of the respective phase stresses according to Eq. 3,

$$\sigma_{L,T,N}^{Macro} = (1-V_f)\sigma_{L,T,N}^{\gamma} + V_f\,\sigma_{L,T,N}^{\alpha} \quad (3)$$

The volume fraction V_f of ferrite was determined from the ASTM E562 point count method.

Intergranular Corrosion Tests (IGC)

A modified ASTM A262 [1] was adopted in conjunction with a modified quantitative test method namely The Double Loop Electrochemical Potentiokinetic Reactivation (DL-ERP) test.

Modified ASTM A262 Standard Practices E—copper–copper sulfate sulfuric acid test for detecting susceptibility to intergranular attack was used. The specimen was covered with copper shot and grindings and immersed in a solution of 16 wt% sulfuric acid with 6 wt% copper sulfate. The solution was then heated to its boiling point and maintained at this temperature for 48 hours. On removal from solution, the specimen was bent through 180° over a rod with a diameter equivalent to twice the thickness of the specimen instead of four times the thickness to ensure, if cracks appeared, they would be apparent by the more restrictive bending radius. The bent surface of the specimen was then examined for cracks at low magnifications in the range X5 to X20.

A modified Double Loop Electrochemical Potentiokinetic Reactivation (DL-ERP) Tests, was used as conducted by Schultz et al. [2,3,4]. The solution used was 0.5M H_2SO_4 + 0.001M TA (thioacetamide). TA is added to reduce the extent of ferrite dissolution. The test was conducted at 60 °C. The polarization scan was started 5 minutes after immersion of the specimen. The potential was scanned from -500 mV (SCE) to +200 mV (SCE) and back to -500 mV (SCE) at a rate of 1.67 mV/s. The ratio of the reactivation charge to the passivation charge was calculated and is shown in the results section.

Magnetic Force Microscopy Analysis

Magnetic force microscopy studies were conducted on metallographically prepared cross-sections of the welds, after grinding and polishing using 3 µm diamond paste. The Scanning Probe Microscopy from Digital Instruments at ANSTO, operating in tapping and lift modes was employed to study the topographic and magnetic features of the DSS samples. Topographic and magnetic force data were taken in the same scan. In order to produce reliable images, repeated scans in different directions were done to ensure reproducibility of the features. Various scan sizes and speeds were tested to enhance height and magnetic induced signals, thus minimizing tip hysteresis and the delay between line scans.

Results and Discussion

The residual stress, microstructure, resulting phase transformation, mechanical properties and degree of susceptibility to IGC are discussed in detail in this section. Table 3 summarises the results of the IGC tests carried out on the welded duplex stainless steels in this study.

Table 3. Summary of the DLERP results of the of the welded duplex stainless steels

Weld Pass	***DL-ERP Test***	
	Qr/Qa	***Ir/Ia***
1 (weld root)	0.04	0.06
2 (weld fill)	-	-
3 (weld fill)	0.09	0.12
4 (weld fill)	-	-
5 (weld cap)	0.04	0.07

Residual Stress Measurements

In the transverse direction, austenite exhibits tensile strains in the weld while the ferrite has contracted lattice spacing. As the distance from the weld centerline increases out to the HAZ (~5mm), an inversion occurs where upon ferrite strains are tensile and austenite is compressive. In the longitudinal direction, the strains for both phases are initially tensile in the weld, although the magnitudes are inverted for each phase in comparison to the transverse direction. In this direction the macroscopic residual stress field is at a maximum, due to constraint impeding contraction of the weld bead during cooling, and it is likely that this is the dominating effect. Moving out from the weld, the HAZ can be clearly distinguished from the weld as both average phase strains become uniformly tensile. This is interesting, in that this area of the weld undergoes transformation back to a completely austenitic structure before transforming partially back to ferrite [5].

In order to convert phase strain to stress (Eq.2) the diffraction elastic constants E_{hkl} and v_{hkl} for each phase must be known, and these in turn depend on the crystallographic texture of the weldment which varies with position from parent to weld. Given the demanding experimental requirement for the texture at each location in the weld, a best approximation of the diffraction elastic constants was chosen using the self-consistent scheme proposed by Kröner [6] for random texture. Such that, E^{α}_{211} = 225.5, E^{γ}_{311} = 183.5 GPa, and ν^{α}_{211} = 0.28 , ν^{γ}_{311} = 0.31 for the ferrite and austenite phases. The calculated phase and macro stresses (Eq.3).

In the normal and transverse direction, the HAZ is strongly tensile for ferrite and compressive for austenite. These results suggest tensile ferrite regions could be susceptible to cracking in the HAZ. It is interesting to note that each phase is under very different stress states throughout the weldment. Considering the samples studied do not have the additive operational stresses normally superimposed on the residual stress field, it is quite likely that ferrite could be subjected to large tensile stresses in practice.

Very high compressive stresses were estimated in the austenite phase for the transverse and normal directions, however, these stresses appear to balance by observation of the macroscopic stress field. It is a requirement for stress balance that the macroscopic stress in the normal direction tend towards zero at the surface and this generally true, however, the magnitude of the compressive stress in the austenite 2mm form the ID surface is questionable. A systematic error in the stress free reference may be a likely source of error.
In the weld, the results show both austenite and ferrite to be under tensile stress in the transverse and longitudinal directions. Observation of the macroscopic stress field shows the highest stress to

occur in the longitudinal (welding) direction as expected. In the transverse direction, where cracking is most problematic in welds, the highest ferrite phase stresses occur in the mid-thickness of the plate.

Microstructural Evaluation and Magnetic Force Microscopy

Microstructural analysis for both GTAW weld conditions as shown by the magnetic force microscopy (MFM) images in Figure 1 reveals the presence of a two-phase banded structure, typical of such materials. In general, the austenite regions observed in the DSS weld metal is formed from ferrite in three modes, viz., as allotriomorphs at the prior-ferrite grain boundaries, as Widmanstätten side-plates growing into the grains from these allotriomorphs and as intragranular precipitates [7]. In the micrographs, the grain boundary allotriomorphs and Widmanstätten austenite are clearly seen. However, the austenite seen within the grain could be either intragranular precipitates or Widmanstätten austenite intercepted transverse to the long axis. These microstructures, in addition to the presence of discontinuous grain boundary austenite layers (Figure 1a) and intragranular acicular ferrite are thought to be associated with variations in transformation rates and the degree of undercooling [8]. In summary, these observed microstructures are typical of those formed under such welding conditions.

The topographic image of (Figure 1d) showed a very flat surface where the only distinguishable features were some contamination particles and a few grinding scratches. From this image, it was not possible to distinguish the distribution of the ferritic and austenitic phases over the surface. On the other hand, the magnetic domain distribution presented in Figures 1a, 1b and 1c are thought to be associated with the microstructures, typical of the various DSS weld regions. The MFM technique was capable of clearly imaging the magnetic domain structure of the ferrite phase that surrounds the “islands” of austenite, appearing flat and uniform due to their paramagnetic properties. Clear bands of ferrite could be easily distinguished, but a closer look revealed other regions of ferrite that did not exhibit the more typical striped magnetic domain configuration, similar to the ferrite regions.

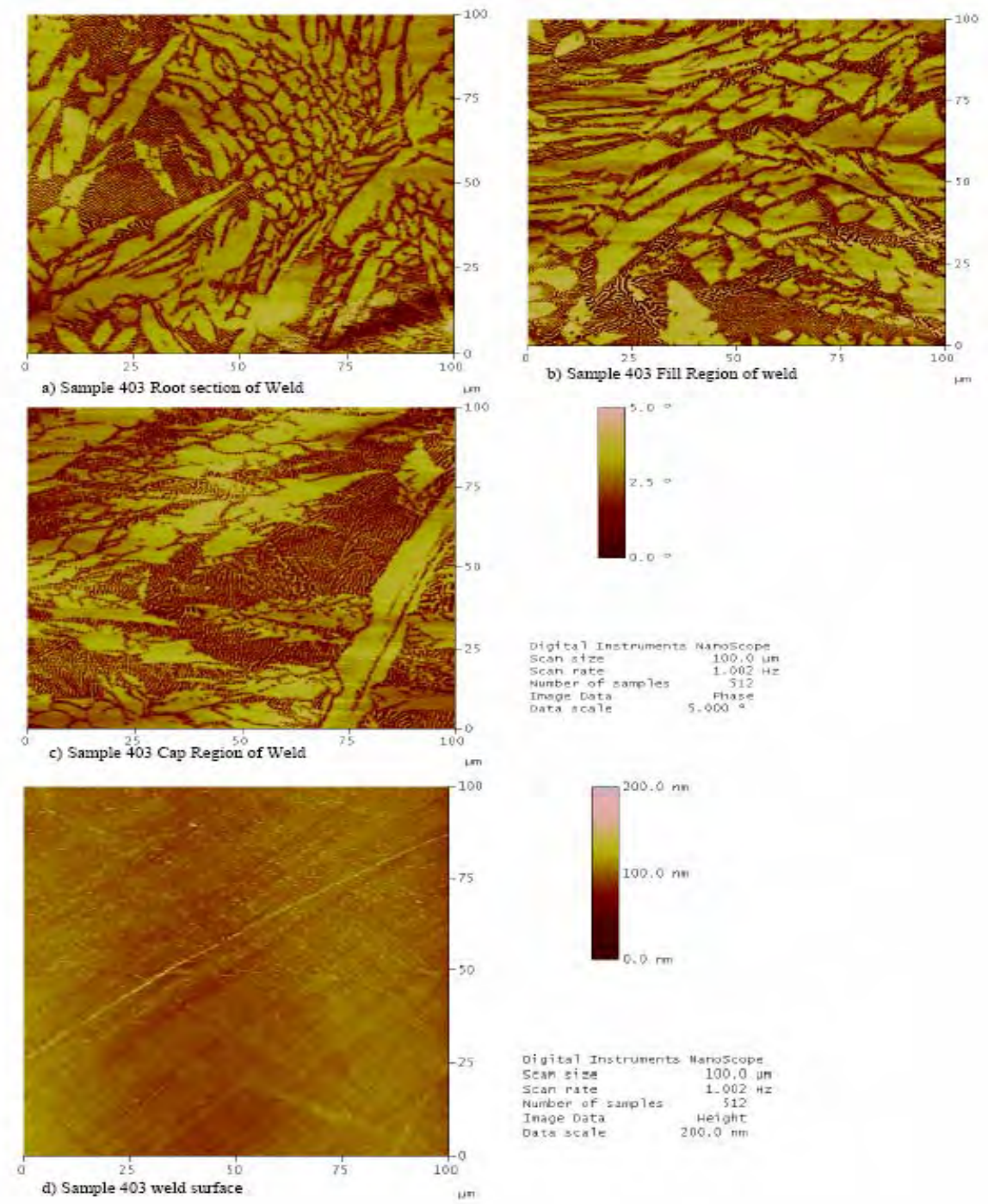

Figure 1. MFM Image of DSS; a) Root region, b) Fill region, c) Cap region, d) Topographical image of weld.

Intergranular Corrosion Tests

Modified ASTM A262 Standard Practices E Test

The absence of cracks on the surface of the bent specimens, even under restricted and reduced bending radius, in accordance with ASTM A262 Standard Practices E, indicates no evidence of sensitization in all weld conditions.

Modified DL-ERP test

The test efficiency was measured by means of a response test, which was characterized by weak values of the current density ratio (Ir/Ia <1%) and the charge ratio (Qr/Qa < 1%) for nonsensitized materials, and relatively high ratio values (Ir/Ia ≥1%) and (Qr/Qa ≥ 1%) for high-sensitized materials. The reverse polarization from the passive to the active region gave rise to a reactivation peak, the magnitude of which is sensitive to the degree of alloy element depletion. The susceptibility to corrosion was characterized in terms of both the ratio of the reactivation-current peak to the activation current peak as well as the ratio of the reactivation charge to the activation charge [9]. Analysis of the results shows that the fill region had a higher degree of sensitization (DOS) compared to the root and cap region of the weld. This correlates with the neutron diffraction measurements of the average phase stress, where tensile ferrite and austenite stresses were observed to be at a maximum in the fill region of the weld in the transverse direction.

Conclusions

- Microstructure of the weld metal as detailed in Figure 1 shows a typical “as weld” structure, resulting in the formation of both fine and coarse structure within the weld metal. This was thought to be associated with variations in transformation rates and the degree of undercooling.
- It was shown the MFM is a powerful tool to use for differentiating the austenite and ferrite phase in duplex stainless steel.
- The DL-ERP test results revealed that the fill area had the highest values for Ir/Ia and Qr/Qa.
- Residual stress measurements by neutron diffraction revealed that the ferrite phase stress was tensile in the HAZ and weld and appeared to be balanced by a local compressive austenite phase stresses in the normal and transverse directions. The results showed that for ferrite and austenite, a maximum tensile stress is formed in the fill section of the weld and decreases in the root and cap regions for the transverse direction.
- A correlation was observed between the stress / strain distribution in the DSS weld regions and the degree of susceptibility to IGC.

References

[1] ASTM A262, Standard Practices for Detecting Susceptibility to Intergranular Attack in Austenitic Stainless Steels.

[2] S. Schultze, J. Gollner, K. Eick, P. Veit, I. Garz, “ The modified EPR test: A new tool for examination of corrosion susceptibility of duplex stainless steel”, Duplex ’97, Paper D97-067, KCI Publishing, Zutphen, The Netherlands (1997), p. 639.

[3] A. Turnbull, P.E. Francis, A.J. Griffiths, E. Bennett, W. Nimmo, “Measurement of Corrosion Resistance of Super-Duplex Stainless Steel Welds by Electrochemical Techniques,” Eurocorr” 2000 (London, U.K.: Institute of Materials, 2000).

[4] E. Otero, C. Merino, C. Fosca, P. Fernandez, “Electrochemical Characterization of Secondary Phases in a Duplex Stainless Steel by EPR Test,” Duplex ’94, paper no. 56 (Cambridge, U.K.: TWI, 1994).

[5] B. Gideon, L. Ward, D. G. Carr “Strain Measurements by Neutron Diffraction and Characterization of Duplex Stainless Steel Welds. Duplex 2007 Conference”, paper 49 (Aquileia and Grado Italy)

[6] E. Kröner, Berechnung der elastischen Konstanten des Vielkristalls aus den Konstanten des Einkristalls, Z. Physik. 151, 1958, p. 404-418.

[7] B. Gideon, L. Ward, G. Biddle, “Testing and Characterization of Duplex Stainless Steel Welds and their Susceptibility to Intergranular Corrosion”, Eurocorr”06, (Maastricht,

Netherlands, September 2006).
[8] L. Karlsson, Welding in the World, Vol. 43, no. 5, 1999.
[9] T. Amadou, C. Braham, and H. Sidhom, Metallurgical and Materials Transactions A, Vol. 35A, Nov. 2004, p. 3499.